

Hypervelocity Stars from the Andromeda Galaxy

Blake D. Sherwin^{1,2*}, Abraham Loeb^{1†} and Ryan M. O’Leary¹

¹ *Harvard-Smithsonian Center for Astrophysics, 60 Garden Street, Cambridge, MA 02138, USA*

² *Department of Applied Mathematics and Theoretical Physics, University of Cambridge, Cambridge CB3 0WA, UK*

15 February 2019

ABSTRACT

Hypervelocity stars (HVSs) discovered in the Milky Way (MW) halo are thought to be ejected from near the massive black hole (MBH) at the galactic centre. In this paper we investigate the spatial and velocity distributions of the HVSs which are expected to be similarly produced in the Andromeda galaxy (M31). We consider three different HVS production mechanisms: (i) the disruption of stellar binaries by the galactocentric MBH; (ii) the ejection of stars by an in-spiraling intermediate mass black hole; and (iii) the scattering of stars off a cluster of stellar-mass black holes around the MBH. While the first two mechanisms would produce large numbers of HVSs in M31, we show that the third mechanism would not be effective in M31. We numerically calculate 1.2×10^6 trajectories of HVSs from M31 within a simple model of the Local Group. Gravitational focusing of the HVSs by the MW and the diffuse Local Group medium leads to high densities of low mass ($\approx 1M_{\odot}$) M31 HVSs near the MW. For both relevant mechanisms, we expect there to be a few thousand solar mass M31 HVSs within the virialized MW halo, many of which should have distinctively large approach velocities ($< -500 \text{ km s}^{-1}$). In addition, we predict ~ 5 hypervelocity RGB stars within the M31 halo which could be identified observationally. Future MW astrometric surveys or searches for distant giants could thus find HVSs from M31.

Key words: stellar dynamics – black hole physics – galaxies: individual: M31 – Local Group

1 INTRODUCTION

Hypervelocity stars (HVSs) travel at such high speeds that they are not gravitationally bound to the galaxy from which they originate. The first HVS was discovered in the Milky Way (MW) halo by Brown et al. (2005); six other HVSs in the MW halo have since been found by Edelmann et al. (2005), Hirsch et al. (2005) and Brown et al. (2006a,b). By selection, most of the observed stars are B-type stars. The HVSs have typical speeds of 550 km s^{-1} . There is also evidence for a bound population of stars similar to the HVSs but with speeds slightly lower than the escape velocity of the MW (Brown et al. 2007). The observations of MW HVSs indicate that all but one of these stars originate from the centre of the galaxy¹. This is easily understood if HVSs are ejected by the massive black holes (MBHs) which inhabit the centres of galaxy bulges.

The ejection of HVSs from galactocentric MBHs was first predicted by Hills (1988). The proposed mechanism

was the disruption of a tight stellar binary by the MBH, which results in the capture of one of the stars and the ejection of the other as a HVS. This tidal breakup (“TB”) mechanism has been further investigated by Yu & Tremaine (2003), Gualandris et al. (2005), Ginsburg & Loeb (2006), and Bromley et al. (2006). Another model for the production of HVSs is the scattering of stars bound to the galactic MBH by an intermediate or high mass in-spiraling black hole (“IBH” mechanism - Yu & Tremaine 2003; Levin 2006; Baumgardt et al. 2006; Sesana et al. 2006, 2007b). Though the results of Sesana et al. (2007a) indicate that this second model may be inconsistent with the statistics of the observed MW HVSs, it cannot be ruled out in M31. The third mechanism for the ejection of HVSs was proposed by O’Leary & Loeb (2006); this involves the scattering of stars by a cluster of orbiting stellar-mass black holes which have segregated around the galactocentric MBH (“BHC” mechanism). It has not yet been conclusively determined which of these mechanisms is dominant in the MW, and so we will consider them all in our work.

The HVSs originating from the MW centre have been studied in some detail by both observers and theorists. However, the production of HVSs is of course not unique to our galaxy; indeed it is expected to be a feature of all galax-

* bds30@cam.ac.uk

† aloeb@cfa.harvard.edu

¹ The HVS discovered by Edelmann et al. (2005) appears to originate from the Large Magellanic Cloud.

ies with central MBHs. The HVSs which escape from other galaxies will become, to quote Hills (1988), “intergalactic tramps”. In particular, the neighbouring Andromeda galaxy (M31) is fairly similar to the MW and has a MBH at its centre (Bender et al. 2005). We thus expect a HVS population similar to that observed in the MW to be produced in M31, with some of the escaping stars gravitationally focused into the MW. Observations of such stars could be used to determine the HVS production mechanism, elucidate the properties and merger history of the core of M31, and constrain the distribution of mass within the Local Group. This leads to two questions which are the subject of our paper: (i) *what is the distribution of stars ejected from M31?*; and (ii) *can we observe them from our galaxy?*

To answer these questions one needs to consider the history of the MW and M31 within the Local Group of galaxies (of which they are the largest constituents). Kahn and Woltjer (1959) first introduced the “timing argument”, by which the MW and M31 are assumed to have formed close to each other in the early universe and were subsequently pulled apart by the general cosmological expansion. The two galaxies are now decoupled from the expansion and have traced out nearly a full Keplerian orbit, which explains the current observed approach velocity of $\approx 120 \text{ km s}^{-1}$ (Binney & Tremaine 1987). Given the current approach velocity, the separation of the galaxies, the age of the universe, and assuming that the Local Group has no angular momentum, one can solve Kepler’s equations to find an estimate of the Local Group mass – $\approx (3\text{--}5) \times 10^{12} M_{\odot}$ (see Binney & Tremaine 1987, Fich & Tremaine 1991). The timing argument has since also been applied to systems with angular momentum and realistic mass distributions (see e.g. Peebles et al. 1989; Valtonen et al. 1993; Peebles 1994; Peebles et al. 2001; Sawa & Fujimoto 2005; Loeb et al. 2005).

The timing argument also allows an approximation to be made about the separation of the MW and M31 for the dynamics of HVSs. A feature of the galaxies’ eccentric Keplerian orbit is that they spend a large fraction of the orbital time near apogalacticon. Since the HVSs move at speeds which are at least a few times larger than the relative radial speeds of M31 and the MW, a reasonable approximation in following the HVS dynamics is to assume that the separation of the MW and M31 has had the current value over the last 10^{10} years.

Recent studies of the Local Group investigated the transverse velocity of M31. Peebles et al. (2001) applied the action principle to the motion of galaxies within 20 Mpc of the Local Group and obtained a transverse velocity of $\approx 200 \text{ km s}^{-1}$. Loeb et al. (2005) analysed the proper motion of M31’s satellite galaxy M33 using numerical simulations and estimated the transverse velocity of M31 as $\approx 100 \text{ km s}^{-1}$. In our work we neglect the transverse velocity as it has only a small influence on the trajectories of the much faster HVSs.

In the following sections we examine the trajectories of HVSs from M31 within the Local Group and estimate their current distribution and observability. We first construct a simple model of the Local Group and its gravitational field as described in §2.1. We then numerically integrate the equations of motion for a large number of possible HVS trajectories ($\approx 10^6$) to find the current HVS distribution within the Local Group, sampling from assumed probability distribu-

tions of HVS ejection direction, ejection speed, and stellar mass, as detailed in §2.2. An analysis of how to perform the simulations most efficiently and a discussion of the numerical methods we use to find the HVS trajectories and distributions is given in §3. The results of our simulations are presented in §4 and discussed in §5. We comment on the observational outlook for our results in §6 and finally conclude in §7.

2 MODELLING THE SYSTEM

2.1 The Local Group

The trajectories and the spatial distributions of the HVSs produced in M31 depend on the gravitational field within the Local Group. A number of models have been constructed of the mass distribution within the entire Local Group (Cox & Loeb 2007) and of the MW and M31 (Klypin et al. 2002; Widrow & Dubinski 2005; Seigar et al. 2006). Much of the Local Group’s mass is contained within the MW and M31 halos. These galaxies are surrounded by a diffuse Local Group medium of dark matter and gas. Based on cosmological simulations in which similar systems form, the mass in the diffuse medium is expected to be a substantial fraction of the total mass (Cox & Loeb 2007); indeed the timing argument’s mass estimate of $\approx (3\text{--}5) \times 10^{12} M_{\odot}$ is generically larger than the sum of the MW & M31 halo masses ($\sim 2.6 \times 10^{12} M_{\odot}$).

We will thus assume in our model that the mass in the intragroup medium is equal within a factor f to the mass contained within the virialized halos of M31 and the MW, $M_A + M_M$. For simplicity, this diffuse Local Group mass is taken to be uniformly distributed within a sphere of radius R_G about the midpoint between M31 and the MW. The two galaxies are separated by 780 kpc (McConnachie et al. 2005, Ribas et al. 2005).

The mass of both the bulge and disc of M31 and the Milky Way is much smaller than the masses of their dark matter halos, so the gravitational influence of the bulge and disc is only important very close to the galaxies’ centres. As we are interested in approximate HVS trajectories and distributions within the entire Local Group and do not require precise trajectories near the galactic centre, we neglect the gravitational field of the disc and bulge in our Local Group model. However, the M31 disc and bulge significantly slow an HVS which is escaping the galactic centre; we take this into account by reducing the HVS initial velocity by an amount which corresponds to the kinetic energy required to escape the disc and bulge. To estimate this reduction in velocity, we assume a Hernquist bulge (Hernquist 1990) with a mass $m_b = 2 \times 10^{10} M_{\odot}$ (Klypin et al. 2002) and a scale radius $a_b = 1.8 \text{ kpc}$ (Widrow & Dubinski 2005), as well as an exponential disc with a mass $m_d = 8 \times 10^{10} M_{\odot}$ and a scale radius $R_d = 5.5 \text{ kpc}$ (Widrow & Dubinski 2005). The central potential of the bulge is $-Gm_b/a_b$ (Widrow & Dubinski 2005), and we calculate the central exponential disc potential to be $-Gm_d/R_d$. The escape velocity v_{bd} from the bulge and disk is thus $v_{bd} \approx 470 \text{ km s}^{-1}$; a HVS with an initial speed v (once outside the influence of the MBH) has a speed $v_0 = \sqrt{v^2 - v_{bd}^2}$ after escaping the bulge and disk. We assume that the gravitational field of the M31 disc does

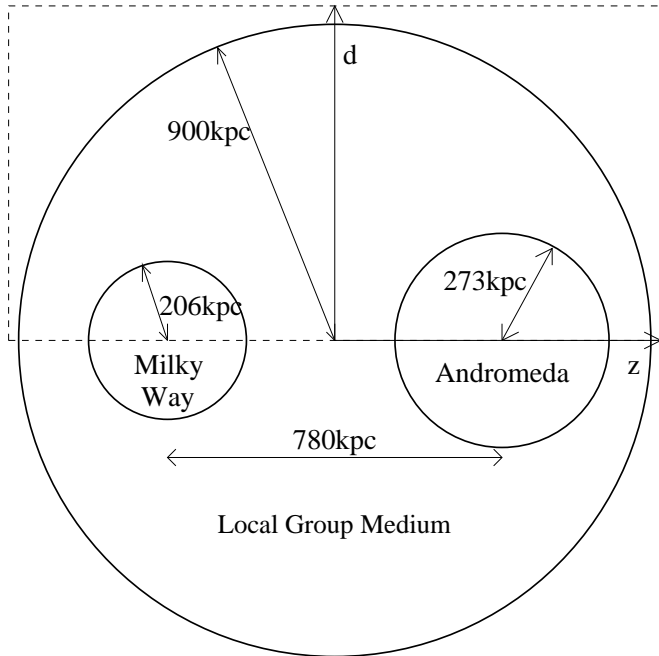


Figure 1. Our model of the Local Group. The dashed line indicates the range of our later plots.

not modify the initial angular distribution of HVSs as the disc’s field is small and mainly radial.

We model the dark matter distribution within the MW & M31 galaxy halos with the Navarro, Frenk and White (1996; hereafter NFW) density profile which follows from cosmological galaxy formation simulations:

$$\rho(r) = \frac{\rho_0}{(cr/R_{200})(1 + cr/R_{200})^2}, \quad (1)$$

where c is the concentration parameter, R_{200} is the virial radius of the galaxy at which we cut off the halos (interior to which the average density is 200 times the mean density of the Universe), and where ρ_0 is a constant chosen to give the correct total virial mass M_A (for M31) or M_M (for MW). The total density in our model is simply the superposition of the densities of the two galaxies and the intragroup medium.

Our Local Group model is thus completely specified by the parameters M_A , M_M , f , $R_{A,200}$, $R_{M,200}$, R_G , c_A and c_M . The standard values of these constants which we use for our model are $M_A = 1.6 \times 10^{12} M_\odot$, $M_M = 1 \times 10^{12} M_\odot$, $f = 1$, $c_A = c_M = 12$, $R_{A,200} = 273$ kpc, $R_{M,200} = 206$ kpc and $R_G = 0.9$ Mpc. These numbers are similar to those in Cox & Loeb (2007), which are based on observations and are also consistent with simulations of the development of the Local Group. The model is depicted in Figure 1. In following the dynamics of fast HVSs near the turnaround epoch of the Local Group, we will assume that the configuration shown in Figure 1 has not changed significantly over the age of the Local Group ($\sim 10^{10}$ yr).

The simplicity of our model enables us to find analytic expressions for the gravitational field, which increases the efficiency of our numerical calculations. Making use of the spherical symmetry of all the features in our model, the gravitational field can easily be calculated from Gauss’ law. Within the Local Group the diffuse mass leads to the field

$$\mathbf{g}_G(\mathbf{r}) = \frac{-G(M_A + M_M)f}{R_G^3} \mathbf{r}.$$

The field within the MW resulting from the NFW halo profile is a central field of magnitude (Navarro et al. 1996)

$$|\mathbf{g}_M(\mathbf{r})| = \frac{GM_M}{R_{M,200}^2} \frac{1}{x^2} \frac{\ln(1+cx) - cx/(1+cx)}{\ln(1+c) - c/(1+c)} \quad (2)$$

where \mathbf{r}_M is the position of the MW centre and $x = |\mathbf{r} - \mathbf{r}_M|/R_{M,200}$. The expression for the M31 field is analogous. The fields have a $1/r^2$ form outside the galaxy or Local Group.

While the halo field is not singular at the centre of the galaxy, we avoid numerical difficulties caused by the denominator by including a softening length $\epsilon R_{M,200}$:

$$\mathbf{g}_M(\mathbf{r}) = -\frac{GM_M}{R_{M,200}^2} \frac{1}{(x + \epsilon)^2} \times \frac{\ln(1+cx) - cx/(1+cx)}{\ln(1+c) - c/(1+c)} \frac{\mathbf{r} - \mathbf{r}_M}{|\mathbf{r} - \mathbf{r}_M| + \epsilon R_{M,200}} \quad (3)$$

We choose a small value of $\epsilon = 0.01$ which introduces a realistic core in the region of the galactic bulge and is found not to influence trajectories away from the galaxy centres.

The total gravitational field is found by superposition:

$$\mathbf{g}_t = \mathbf{g}_G + \mathbf{g}_M + \mathbf{g}_A.$$

2.2 The HVS Production Rate

To accurately model the ejection of HVSs from M31, we must determine the number of HVSs produced, the probability distribution of the HVSs’ initial velocities, and the distribution of their stellar masses. For simplicity, we will assume that HVSs have been ejected in the same manner throughout the lifetime of the Local Group; the velocity and mass probability distributions are thus assumed constant over the last 10^{10} years, with no HVS production before this time. We neglect the possibility that multiple mechanisms simultaneously contribute to the HVS production and only consider the mechanisms individually.

We first discuss the number of HVSs produced in the MW. A HVS production rate in the MW can be estimated by extrapolating the observations of hypervelocity blue stars in the MW halo to lower masses. We assume that star formation in the MW galactic centre has followed a flat initial mass function $\frac{dN}{dm}$ as found in current observations of the galactic centre, $\frac{dN}{dm} \propto m^{-0.85}$ for $m \geq 1M_\odot$ (Maness et al. 2007). The cumulative distribution of stellar masses in the galactic centre $P(m)$ is given by $P(m) \propto \frac{dN}{dm} t_l$ (see Alexander & Sternberg 1999, O’Leary & Loeb 2007, Sesana et al. 2007a, Perets et al. 2007). This implies that $P(m) \propto m^{-3.35}$, where t_l is the stellar lifetime, which is less than a Hubble time, and we have used $t_l \propto m^{-2.5}$ (Kippenhahn & Weigert 1990). Taking the masses of ejected HVSs to be distributed according to $P(m)$ and assuming that HVSs were produced at a constant rate, the limited HVS sample of Brown et al. (2006a) leads to a rough estimate of slightly more than 10^6 HVSs ejected from the MW centre over the age of the local group.

The number of HVSs produced in M31 will not necessarily be the same as the number produced in the MW. While M31 is overall very similar to the MW, the masses of the MBHs in the galaxies are very different; the mass

of the MW’s MBH (Sgr A*) is $\approx 3.6 \times 10^6 M_\odot$ (Eisenhauer et al. 2005), whereas the mass of the MBH in M31 is $\approx 1.4 \times 10^8 M_\odot$ (Bender et al. 2005). In addition, the stellar populations in the centres of the two galaxies have different velocity dispersions, mass functions and densities (Bender et al. 2005, Genzel et al. 2003). As the MBH and its stellar environment play a large role in all HVS production mechanisms, we must investigate how the differences will influence the relative HVS production rates in the MW and in M31. We can then simply scale the rates in the MW (inferred from observations) for each of the mechanisms to obtain the total number of HVSs produced in M31.

We briefly review some features of the stellar environment of MBHs. The stars in the galactic centre have a typical mass $m_s \sim 1M_\odot$. The radius of influence, r_i , is the distance to which the MBH significantly influences the velocity and spatial distribution of stars; at this radius the kinetic energy in the random motions of the stars (characterised by the velocity dispersion σ) is roughly equal to the stars’ potential energy in the gravitational field of the MBH, so that $r_i \approx GM_\bullet/\sigma_i^2$, where M_\bullet is the mass of the central MBH. Outside the radius of influence, σ is approximately constant with radius ($\sigma \approx \sigma_i$); inside the radius of influence, the velocity dispersion roughly equals the circular velocity ($\sigma(r) \approx \sqrt{GM_\bullet/r}$). The density of stellar mass near the black hole is assumed to be described inside the radius of influence by the theoretically derived expression (Young 1980):

$$\rho(r) = \rho_i(r/r_i)^{-1.5}. \quad (4)$$

Outside the radius of influence, we assume an isothermal stellar distribution, so that

$$\rho(r) = \rho_i(r/r_i)^{-2}. \quad (5)$$

While one could also determine a density profile based solely on current observations and not on theoretical considerations, the current density would not necessarily correctly describe the density over the past 10^{10} years; we believe that the above theoretical expressions for the density should provide a better average model over the age of the Local Group. Our density profile agrees fairly well with observations of the galactic centres of both the MW (Genzel et al. 2003) and M31 (Lauer et al. 1993). We use the following values of r_i , ρ_i and σ_i (assuming a density profile as in Eq. 4): for the MW $r_M = 1.66\text{pc}$, $\rho_M = 6 \times 10^4 M_\odot/\text{pc}^3$ and $\sigma_M \approx 100 \text{ km s}^{-1}$ (Genzel et al. 2003); for M31 $r_A = 30\text{pc}$, $\rho_A = 6 \times 10^2 M_\odot/\text{pc}^3$ and $\sigma_A \approx 150 \text{ km s}^{-1}$ (Bender et al. 2005, Lauer et al. 1993). We assume a binary fraction η of $\eta = 0.1$.

In the BHC model, a cluster of stellar-mass black holes has segregated close to the MBH. The stars near the MBH are moving at high speeds, so that scattering of these stars off the orbiting stellar-mass black holes leads to hypervelocity ejections. The BHC mechanism of course presupposes that the stellar-mass black holes have had sufficient time since the formation of the galaxy to segregate into a central cusp. The segregation occurs by dynamical friction on the timescale $t_d \approx \frac{m_s}{m_b} t_r$, where t_r is the relaxation timescale

$$t_r(r) = 0.34 \frac{\sigma(r)^3}{G^2 m_s \rho(r) \ln \Lambda} \quad (6)$$

(Binney & Tremaine 1987), $m_b \sim 7M_\odot$ is the mass of a

typical segregating black hole and $\ln \Lambda$ is the Coulomb logarithm which we take as ≈ 10 . Using the expressions for density and velocity dispersion above, it is easily shown that the relaxation and dynamical friction timescales have a constant minimum value below the radius of influence and rise as r^2 outside it. Thus we can calculate the minimum time required to form a cluster of black holes from the minimum dynamical friction timescale at the radius of influence $t_d(r_i)$. For the MW, the minimum dynamical friction timescale is $t_M \approx 1.4\text{Gyr}$ (Miralda-Escudé & Gould 2000) which implies that a black hole cusp would form within a small fraction of the age of our galaxy and produce HVSs. Equation (6) implies that the minimum dynamical friction timescale in M31 is

$$t_A = t_M \left(\frac{\sigma_A}{\sigma_M} \right)^3 \left(\frac{\rho_M}{\rho_A} \right) \quad (7)$$

which gives $t_A \approx 340t_M \approx 480\text{Gyr}$. This greatly exceeds the age of the universe, and it follows that no central black hole cluster has formed in M31². We thus do not expect any HVS production in M31 by the BHC mechanism, and we will not consider this mechanism in our calculations.

We now consider the effect of the increased MBH mass and different stellar environment in M31 on the TB mechanism. In the TB mechanism, a binary which approaches the MBH to within the tidal radius r_t is disrupted; one of the stars is captured and its binary companion is ejected at high velocity. A binary will be disrupted within an orbital period t_p if its orbital specific angular momentum (per unit mass) j is sufficiently small, $j \leq j_{min} \approx \sqrt{GM_\bullet r_t} \approx \sqrt{GM_\bullet a (M_\bullet/m_s)^{1/3}}$, where a is the binary separation. This range corresponds to a region in the angular momentum – energy phase space which is known as the “loss-cone”. The rate of binary disruption is either limited by the orbital period (“full loss-cone”) or by the time for binaries to diffuse into the loss cone (“empty loss cone”); to calculate the total rate one must consider both these regimes (see Frank & Rees 1976, Lightman & Shapiro 1977, Cohn & Kulsrud 1978, Magorrian & Tremaine 1999, Yu & Tremaine 2003 and Perets et al. 2007). The cross-over from the empty to full loss-cone regimes occurs at a critical radius r_c where the root-mean-square angular momentum change Δj due to stellar encounters during one orbital period t_p is equal to j_{min} . We can calculate the critical radius as follows. r_c is defined by

$$\Delta j(r_c) = j_{min}. \quad (8)$$

The root mean square specific angular momentum transfer over one orbital period is (Lightman & Shapiro 1977)

$$\Delta j \approx \left(\frac{t_p}{t_r} \right)^{1/2} j_{circ}, \quad (9)$$

where $j_{circ}(r) \approx \sigma(r)r$ is the specific angular momentum of a star on a circular orbit. This implies

² A caveat to this conclusion involves violent relaxation (Lynden-Bell 1967) which could result from a merger event. However, the effect of a merger is expected to be episodic and would not lead to a cumulative segregation process that is considered here over long periods of time.

$$\left(\frac{j_{min}}{j_{circ}(r_c)}\right)^2 \approx \frac{t_p(r_c)}{t_r(r_c)}. \quad (10)$$

Noting that within the radius of influence σ is of order the circular velocity and that outside the radius of influence it is a constant, we take $t_p \approx 2\pi r/\sigma(r)$. Using the expressions given previously for j_{min} , j_{circ} and t_r , we obtain an equation involving r_c

$$\frac{GM_\bullet a(M_\bullet/m_s)^{1/3}}{\sigma^2(r_c)r_c^2} \approx \frac{2\pi r_c G^2 m_s \rho(r_c)}{0.034\sigma^4}. \quad (11)$$

Solving this equation using $a = 0.1\text{AU}$ leads to a critical radius significantly larger than the radius of influence for both M31 and the MW ($r_i/r_c \ll 1$).

We now make an order of magnitude estimate of the HVS production rates using our density profile. As is discussed in Perets et al. (2007) §4, the contribution to the total rate Γ is $d\Gamma/dr \propto r^{1/2}$ for $r < r_i$, $d\Gamma/dr \propto r^{-2}$ for $r_i < r < r_c$ and $d\Gamma/dr \propto r^{-3}$ for $r > r_c$. The continuity of $d\Gamma/dr$ allows us to estimate the relative contributions of these three different regions to the total rate; it is easily shown that the contribution from the full loss-cone region $r > r_c$ is smaller than that from the empty loss cone region $r < r_c$ by a factor r_i/r_c and is thus negligible. Perets et al. (2007) give an approximate expression for $d\Gamma/dr$ in the empty loss cone regime (their Eq. 17):

$$\frac{d\Gamma_e}{dr} \sim \frac{N_s(< r)}{rt_r(r_c)} \quad (12)$$

where $N_s(< r)$ is the number of binaries enclosed within r . The total rate can thus be obtained from an integration over r :

$$\Gamma \sim \int_0^{r_c} \frac{d\Gamma_e}{dr} dr \sim \int_0^\infty \frac{d\Gamma_e}{dr} dr \sim \frac{40\pi G^2 \eta \rho_i^2 r_i^3}{0.034 \times 6\sigma_i^3} \quad (13)$$

Equation (13) allows us to find the expected ratio of HVS production in the MW and M31 based on the observational data mentioned above³:

$$\frac{\Gamma_A}{\Gamma_M} \sim \left(\frac{\rho_A}{\rho_M}\right)^2 \left(\frac{r_A}{r_M}\right)^3 \left(\frac{\sigma_M}{\sigma_A}\right)^3 \sim 0.2 \quad (14)$$

This rough estimate indicates that the TB mechanism produces 1–10 times fewer HVSs in M31 than in the MW.

The IBH mechanism is also affected by the differences between the MW and M31. The HVS ejection rate was calculated for M31 by Lu et al. (2007) by adopting the method of Yu & Tremaine (2003); assuming an IBH/MBH mass ratio of $\nu = 0.01$ and an IBH-MBH axis of 5.9mpc the rate is approximately an order of magnitude lower than in the MW (of order $10^{-5}/\text{yr}$).

To summarise, the BHC mechanism produces no HVSs in M31, and both the TB and IBH HVS production rates are suppressed in M31 by a factor of order 1–10 compared to the MW. However, this may be partially compensated for by the somewhat higher ejected star velocities in M31 (Yu & Tremaine 2003) which decrease the proportion of bound ejected stars. The number of HVSs produced over the past 10^{10} years in the MW is expected to be somewhat above

10^6 . For our calculations with both these mechanisms we thus assume that the total number of HVSs produced in M31 is 10^6 . This estimate is fairly uncertain and relies on the assumptions that the stars are isotropically distributed and that the effects of any massive perturbers (Perets et al. 2007) are equal in the MW and in M31. The number of HVSs produced could easily be an order of magnitude lower or higher than our estimate. However, our statistical results can be simply scaled to a different number of ejected stars based on future observations and calculations.

2.3 HVS Velocities and Masses

We now consider the probability distributions for the HVSs' ejection velocities and masses. Both the TB and IBH models have the welcome feature that the form of the probability distribution for the velocity of an ejected star is at most weakly dependent on its mass: for the IBH mechanism, the velocity is entirely independent of the mass of the HVS (as the HVS acts as a test particle in the gravitational field of the much heavier black holes); for the TB mechanism, the velocity of a HVS of mass m_1 shows a very weak dependence $\propto \sqrt{m_2}(m_1 + m_2)^{-1/6}$, where m_2 is the mass of the other binary component (Hills 1988). We thus approximate the velocity and mass distributions as independent, which makes our numerical exploration of their statistics much simpler.

For the TB model, Sesana et al. (2007a) apply the results of Bromley et al. (2006) to binaries with a semi-major axis a distributed uniformly in $\ln a$ (Heacox 1998). Following their Figure 1 (TBf model), the TB mechanism gives rise to a distribution of star ejection velocities v (after escaping the gravitational field of the MBH) of approximately

$$P(v) \propto \begin{cases} v^{-4.9}, & v \geq v_l \\ 0, & v < v_l \end{cases} \quad (15)$$

where $P(v)dv$ provides the probability that a star has an ejection speed in the interval $(v, v + dv)$. While this velocity distribution was derived for the MW, we will assume that the power law index of the distribution is characteristic of the HVS production mechanism and does not depend strongly on the MBH mass, so that this distribution can also be applied to M31. v_l is the lower cutoff velocity, which we define as the maximum speed with which stars do not escape the M31 halo over 10^{10} years for any ejection direction. v_l is thus very similar to (but slightly smaller than) the escape velocity.

The HVS velocity distribution for the IBH model was calculated numerically for the MW by Sesana et al. (2006, 2007a,b). With an IBH/MBH mass ratio of $\nu = 1/729$ and an initial orbital eccentricity of $e = 0.9$, they consider the entire in-spiral of the black hole and obtain a HVS velocity distribution $\propto v^{-2.5}$. We will again assume that the M31 HVS ejection velocity distribution has the same power law index as was found in the MW and thus obtain for M31

$$P(v) \propto \begin{cases} v^{-2.5}, & v \geq v_l \\ 0, & v < v_l \end{cases} \quad (16)$$

As explained previously, the initial speed v_0 we use for our simulations of HVS trajectories is given by $v_0 = \sqrt{v^2 - v_{bd}^2}$ (taking into account the slowing by the M31 bulge and disc.)

Neither the TB nor the IBH mechanisms preferentially

³ We also verified that this simple formula gives a rate very similar to the more exact Yu & Tremaine 2003 calculation for the MW.

eject stars of a certain mass, and so the distribution of ejected stellar masses follows the distribution of main sequence stars in the galactic centre. However, the star formation history in M31 over the past 10^{10} years is not known, and so for simplicity we will assume a Salpeter initial mass function $\frac{dN}{dm} \propto m^{-2.35}$. As observations indicate that the formation of low mass stars is suppressed in galactic centres (Maness et al. 2007), we cut off the mass distribution below $1M_{\odot}$. As discussed previously, taking stellar lifetime into consideration implies that the HVSs ejected from M31 thus have masses distributed according to

$$P(m) \propto \begin{cases} m^{-4.85}, & m \geq 1M_{\odot} \\ 0, & m < 1M_{\odot} \end{cases} \quad (17)$$

We assume that the HVSs are ejected isotropically from the M31 centre.

3 NUMERICAL METHODS AND ANALYSIS OF OUR MODEL

3.1 Numerical Methods

In order to obtain HVS distributions and velocities we must simulate a large number of individual stellar trajectories. The basic challenge of this calculation is to integrate Newton’s gravitational force law. The integration method we use is the Verlet method (Verlet 1967), which has a number of advantages: it is symmetric (i.e. it uses information from both ends of a step), it is a fourth order method, and it is sufficiently fast to allow a large number of trajectories to be calculated; many HVS trajectories are needed to obtain statistically valid information. A fixed step size is used for our integration as this greatly simplifies the determination of the HVS distributions.

To find one HVS trajectory, our integrator was run for a time corresponding to the age of the Local Group, which we take to be 10^{10} years. We tested our program by comparing its results with a number of analytically calculated trajectories for different force laws. Our numerical results agreed with the analytical solutions for all the configurations we tested (e.g. Keplerian orbits, simple harmonic motion). For our numerical simulations, we chose to use 10^4 integration steps per trajectory. This number of steps was not computationally expensive and gave results which agreed very well with analytic solutions. It was verified that the trajectories were identical for a wide range of step-numbers (from 500 to 2×10^5), which suggests that the integration scheme is stable and that our results are reliable.

3.2 Symmetry Considerations

Our model for the Local Group has a number of important symmetries, which can be exploited to make the necessary numerical calculations more efficient. As is seen in Figure 1, the system exhibits rotational symmetry along the z axis connecting the two galaxies, which means that every trajectory of an HVS from the centre of M31 follows a path which lies in a single plane through the inter-galactic axis. This feature allows us to reduce our problem from three to two dimensions (and thereby increase the computational efficiency), by “folding” all possible trajectories into one cross-

section plane within which we perform all our calculations. To regain three dimensional results we can simply deproject our values. An isotropic ejection in three dimensions corresponds to the following distribution in two dimensions:

$$P(\theta) = \frac{1}{2} \sin \theta \quad (18)$$

where θ is the angle between the intergalactic z -axis and the initial HVS velocity vector.

In addition, the reflection symmetry of the upper and lower half planes means that a “reflected” trajectory is also a valid one. We can thus limit ourselves to sampling trajectories that begin in the upper half plane.

The final and most important symmetry involves time. In our model the mass distribution as shown in Figure 1 is static. This means that every point (not just the endpoint) of a trajectory is a possible current location of a HVS. For every simulated trajectory we thus obtain not one, but many possible current star positions.

The choice of a two-dimensional static Local Group model over a three-dimensional dynamic model reduces the computational time for the HVS distributions by a factor of 10^7 .

3.3 Calculation of the HVS Distributions

To find the HVS distributions and velocities, we must calculate a large number of HVS trajectories. The initial conditions for each trajectory are determined by sampling randomly from the distributions for the HVS ejection angle (Eq. 18) and speed (Eq. 15/16). We use Park and Miller’s (1988) “Minimal Standard” random number generator together with the transformation method detailed in Press et al. (1996) to obtain initial conditions with the required distribution. 1.2×10^6 trajectories were thus calculated, which correspond to 1100 independent samples in both angle and velocity. For each trajectory we used 10^4 timesteps. This means that we obtain a total of 1.2×10^{10} points, each of which is a possible current position of a HVS. However, due to the finite stellar main-sequence lifetime, each of these points does not carry equal weight when determining the distribution of HVSs within the Local Group.

We now consider how to obtain the distribution of HVSs from the raw trajectory data. The lifetime t_l of a star of mass m is assumed to be $t_l = 10\text{Gyr}(m/M_{\odot})^{-2.5}$ (Kippenhahn & Weigert 1990). We take the age of the Local Group to be $t_{\text{age}} = 10^{10}\text{yr}$. Every point on a trajectory corresponds to an HVS travel time t_t which can range from zero to t_{age} . Before being ejected from the centre of M31, a star is assumed to have resided in the galactic centre for a “dwell time” t_d . For a star with mass m and corresponding main-sequence lifetime t_l , a point along a trajectory corresponding to a travel time t_t can contain a “live” star if $t_t + t_d \leq t_l$. Therefore the probability $F(t_t)$ of a star at a point corresponding to t_t being “live” is equal to the probability that $t_d < (t_l - t_t)$.

To determine this probability we must consider the distribution of dwell times $P(t_d)$. There are two conditions on t_d . A “live” star cannot have resided in the galactic centre for more than its main-sequence lifetime t_l , so that $t_d < t_l$. Of course, it can also not have been there before the formation of the Local Group $t_{\text{age}} = 10^{10}$ years ago, which implies $t_d + t_t < t_{\text{age}}$. Thus the maximum value of t_d is

$t_{d,\max} = \min(t_l, t_{\text{age}} - t_t)$. We assume that a live star is equally likely to have been in the galactic centre for any time up to the maximum permissible value $t_{d,\max}$, and the dwell time thus obeys a uniform probability distribution $P(t_d) = 1/t_{d,\max}$ between 0 and $t_{d,\max}$.

The probability $F(t_t)$ of a star at a point with a travel time t_t being live is equal to the likelihood of fulfilling the condition $t_d < (t_l - t_t)$, i.e.

$$F(t_t) = \int_0^{t_l - t_t} P(t_d) dt_d \quad (19)$$

The different ranges of this integral imply different forms for $P(t_d)$, which complicates this (otherwise straightforward) integral. If $t_l < 0.5t_{\text{age}}$

$$F(t_t) = \begin{cases} 1 - \frac{t_t}{t_l}, & t_t < t_l \\ 0, & t_t > t_l \end{cases} \quad (20)$$

If $t_l > 0.5t_{\text{age}}$

$$F(t_t) = \begin{cases} 1 - \frac{t_t}{t_l}, & t_t < t_{\text{age}} - t_l \\ 1 - \frac{t_{\text{age}} - t_l}{t_{\text{age}} - t_t}, & t_l > t_t > t_{\text{age}} - t_l \\ 0, & t_t > t_l \end{cases} \quad (21)$$

The density of HVSs within the Local Group is thus calculated as follows. We partition the ejected stars into six mass bins containing equal numbers of HVSs according to the mass distribution given by equation (17). The mass ranges corresponding to these bins are $(1 - 1.05)M_\odot$, $(1.05 - 1.11)M_\odot$, $(1.11 - 1.20)M_\odot$, $(1.20 - 1.33)M_\odot$, $(1.33 - 1.59)M_\odot$ and $(> 1.59)M_\odot$ for mass bins one through six. The average mass in each bin is used to determine the corresponding t_l , which allows the calculation of $F(t_t)$ for all values of t_t . We then divide the upper half plane of Figure 1 into an array of (300×600) cells and add up the number of points in each cell, with each point weighted by $F(t_t)$. Dividing by the total number of trajectory points ($1.2 \times 10^6 \times 10^4$) as well as the volume corresponding to each cell and multiplying by the total number of HVSs produced gives a number density $n(d, z)$ of stars/kpc³ for each mass bin; the coordinates (d, z) are defined in Figure 1.

In addition to the distributions for the six mass bins, we also consider heavy stars with masses above $3M_\odot$. These are important observationally due to their high luminosity (the observed MW HVSs have mainly been 3–4 M_\odot stars). We take their lifetime to be represented by $t_l = 0.35\text{Gyr}$ (Schaller et al. 1992).

4 RESULTS

4.1 Star Trajectories

We first investigated the shapes and characteristics of individual star trajectories. Single HVSs were expelled from the centre of M31 with a variety of initial conditions and their subsequent paths were found by integration of the gravitational force. For large ejection velocities ($v > 900 \text{ km s}^{-1}$) the stars escaped the Local Group entirely, without being deflected significantly from their original straight trajectories. For velocities smaller than the lower cutoff velocity, the stars were bound to M31 and precessed about its centre in loop orbits. In addition to the bound and expelled stars, stars

released under certain angles with a small range of velocities $\approx 650 - 900 \text{ km s}^{-1}$ were gravitationally pulled into the MW or towards the intergalactic axis. Their trajectories had very low average speeds of approximately $100 - 200 \text{ km s}^{-1}$, as these stars have just enough energy to escape M31's attraction and thus spend a large amount of time at a low velocity.

The value of the lower cutoff velocity was determined as follows. We ejected a large number of stars out of the centre of M31 with a fixed speed but in different directions, and observed whether or not all stars remained within the M31 halo over the age of the Local Group. Stars released towards the centre of the Local Group escaped M31 with lower velocities than ones released away from the centre. By trial and error, we were able to determine that the highest speed at which all stars remained bound was $v_l = 650 \text{ km s}^{-1}$.

An interesting feature of the system emerged during our analysis. It was found that the shape of the trajectories was very sensitive to the initial conditions for some parameter values. In some cases, a change of less than one percent in the starting velocities lead to the ejected stars following entirely different trajectories. While the paths with slightly different starting conditions were identical initially, it was found that the trajectories split after a certain time. These characteristics are indicative of chaotic behaviour in some regions of phase space. It was found that such chaotic behaviour was most common for trajectories which passed through the region between the two galaxies. The chaotic sensitivity to boundary conditions appeared to require the presence of three gravitating objects (the two galaxies and the diffuse group medium); when only two of these objects were present, the system no longer showed chaotic behaviour.

While it is difficult to make precise calculations of the trajectories of individual stars in a chaotic system, our numerical experiments demonstrated that statistical properties, such as HVS spatial and velocity distributions, were not sensitive to slight changes in the initial conditions.

4.2 HVS Spatial Distributions

To determine whether the HVSs from M31 are observable, it is necessary to find the HVS distribution within the Local Group. By integrating 1.2×10^6 trajectories numerically and processing the points on the trajectory as described previously, the HVS distributions were found for both the TB and IBH mechanisms. We obtain distributions and average radial and transverse velocities for all six mass bins and the heavy stars; Figures 2, 3, and 4 show the results for the first, third and fifth mass bins respectively. Distributions and velocities for the $(> 3M_\odot)$ stars are depicted in Figure 5.

The plots of the HVS distributions in Figures 2–4 exhibit a number of interesting features. We first consider the TB mechanism mass bins (left columns of Figs. 2, 3, 4). It is clear that especially for the lower mass stars, the HVS number density departs significantly from an isotropic distribution. For the low mass stars of the first bin, there is a sharp-featured arc of increased number density ($n \sim 10^{-5}/\text{kpc}^3$, roughly 10 times the background density) which extends from M31 to the region behind the MW. In addition, the star density is very high on axis ($\approx 10^{-3}/\text{kpc}^3$); this leads to an average density of first-mass-bin stars in the MW of $\approx 10^{-4} - 10^{-3} \text{ kpc}^{-3}$. For higher mass stars, the deviations

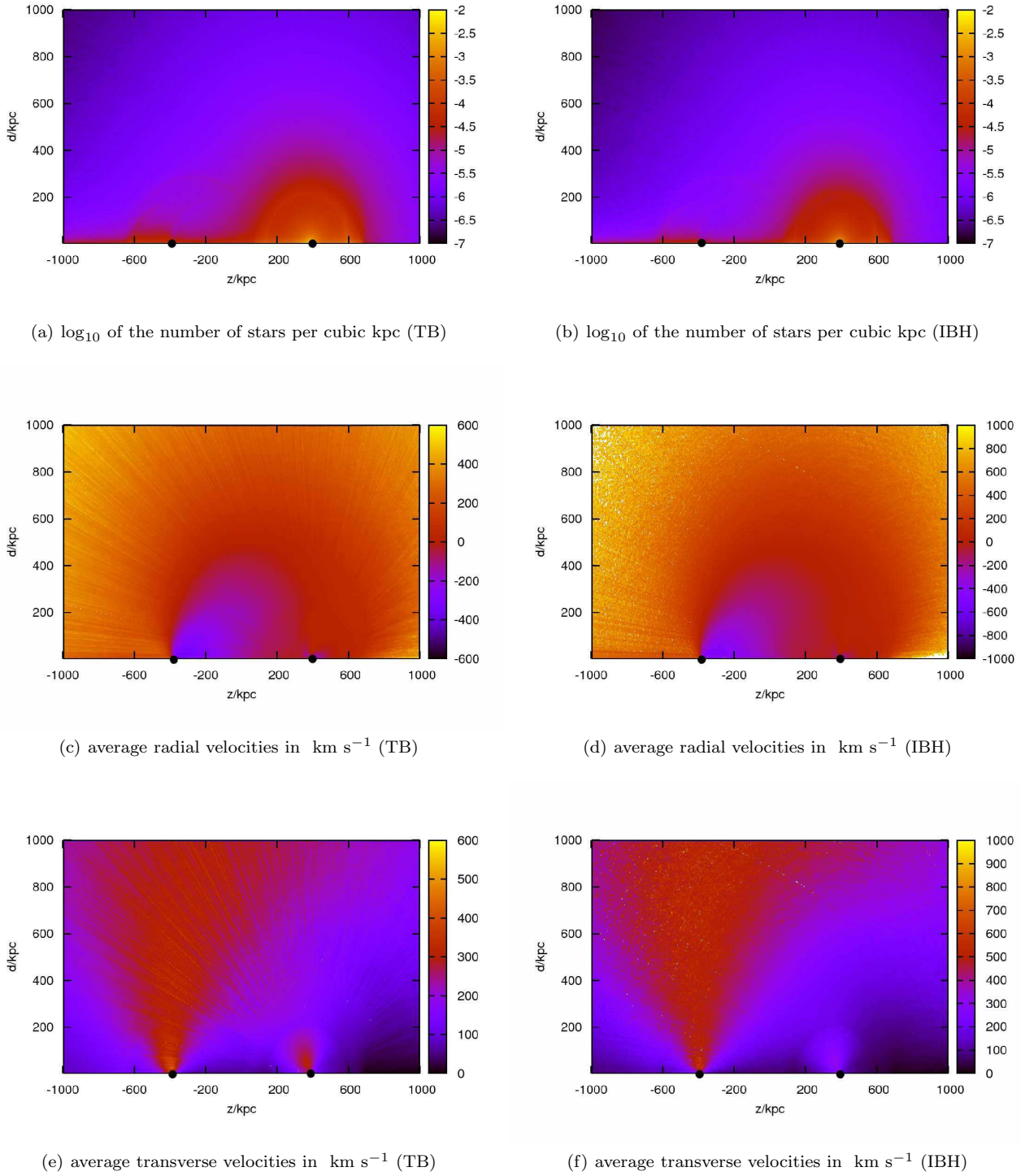


Figure 2. Main-sequence HVS number densities, radial velocities and transverse velocities (with respect to the MW galactic centre) for stellar masses of $(1-1.05)M_{\odot}$. Plots are shown for the TB mechanism (*Left column*) and the IBH mechanism (*Right column*). White colour indicates a value off the scale on the bar to the right of the plots. The positions of the MW and M31 centres are marked with black dots, with the MW on the left. See Figure 1 for the definition of the (d, z) coordinates.

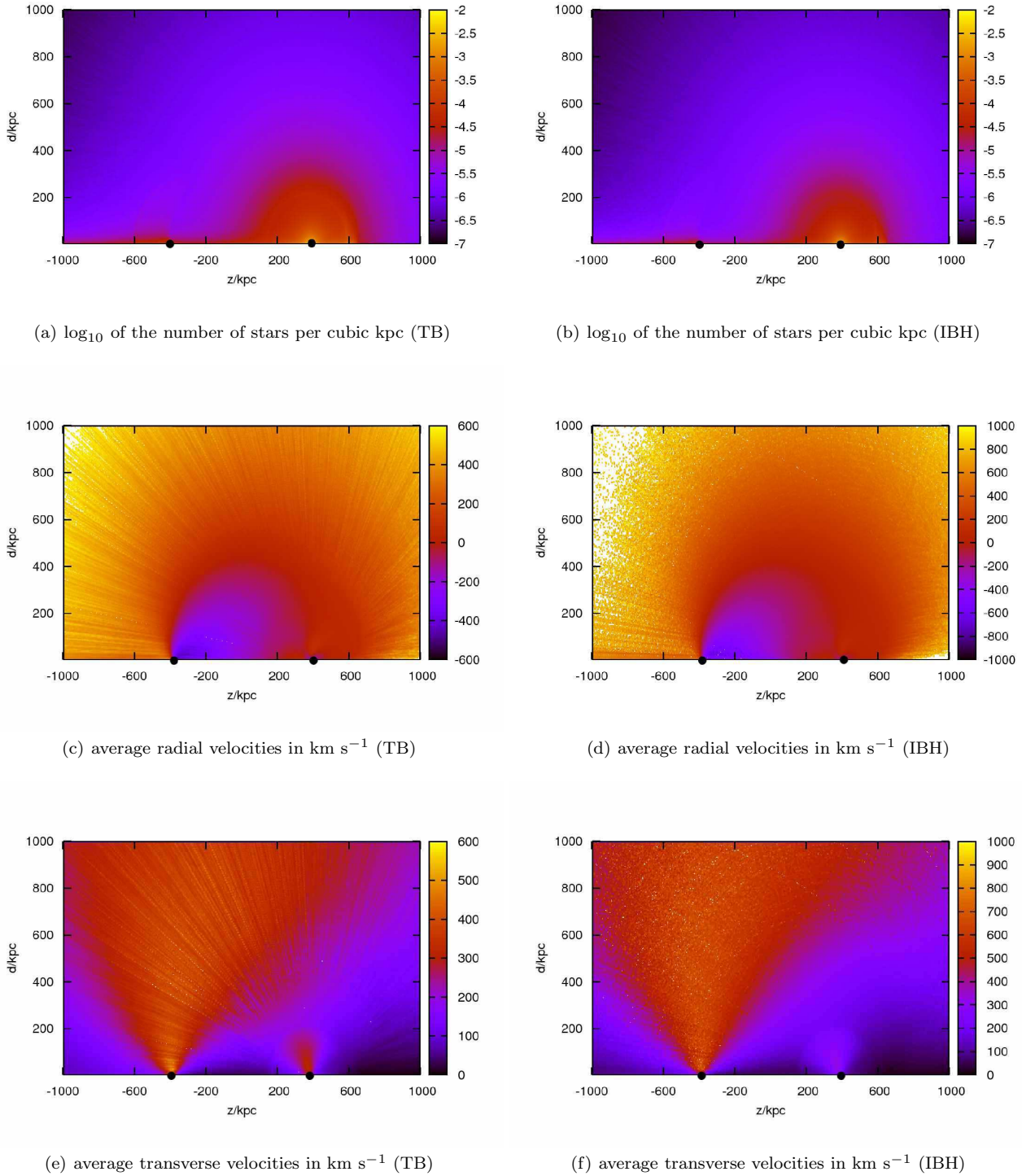


Figure 3. Same as Fig. 2 for stellar masses of $(1.11\text{--}1.20)M_{\odot}$.

from isotropy are smaller: for the third mass bin, the arc of raised probability is hardly visible and the axial maximum is less pronounced; for the fifth mass bin, the HVS distribution is almost entirely isotropic. Another feature which is (barely) visible in these plots is the presence of shell-like peaks in density around M31. While shell-like features are often seen in galaxy merger simulations (e.g. Hernquist &

Quinn 1989), changing our velocity distribution showed that these shells were an artificial feature due to the sharp cutoff in the lower ejection velocity. The density of the $\geq 3M_{\odot}$ stars (Fig. 5) was found to fall off quickly and isotropically with distance from M31. The density is $10^{-6}/\text{kpc}^3$ at a distance of $\approx 200\text{kpc}$ from M31, and only $10^{-9}/\text{kpc}^3$ at a distance of $\approx 500\text{kpc}$.

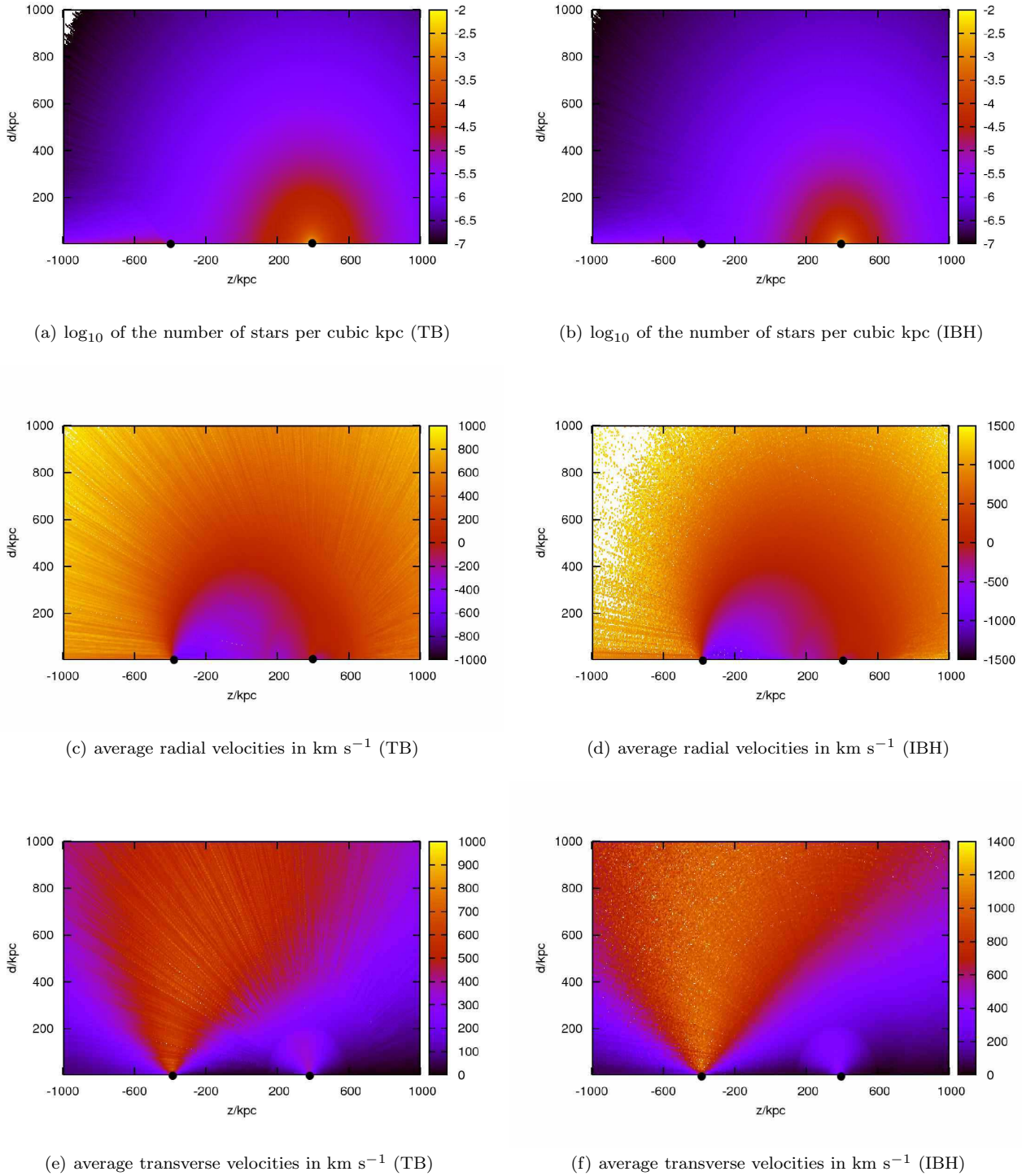


Figure 4. Same as in Fig. 2 for stellar masses of $(1.33 - 1.59)M_{\odot}$.

The lower-mass HVS distributions for the IBH mechanism (right columns of Figs. 2, 3, 4) are very similar to the corresponding plots for the TB mechanism, with only small differences. It can be seen that the arc of first-mass-bin stars is less pronounced for the IBH mechanism. The distribution of the $\geq 3M_{\odot}$ stars is significantly different from the TB mechanism distribution. For the IBH mechanism, the den-

sity of these stars falls off much more slowly with distance to give a value of $10^{-9}/\text{kpc}^3$ at a distance from M31 of $\approx 800\text{kpc}$.

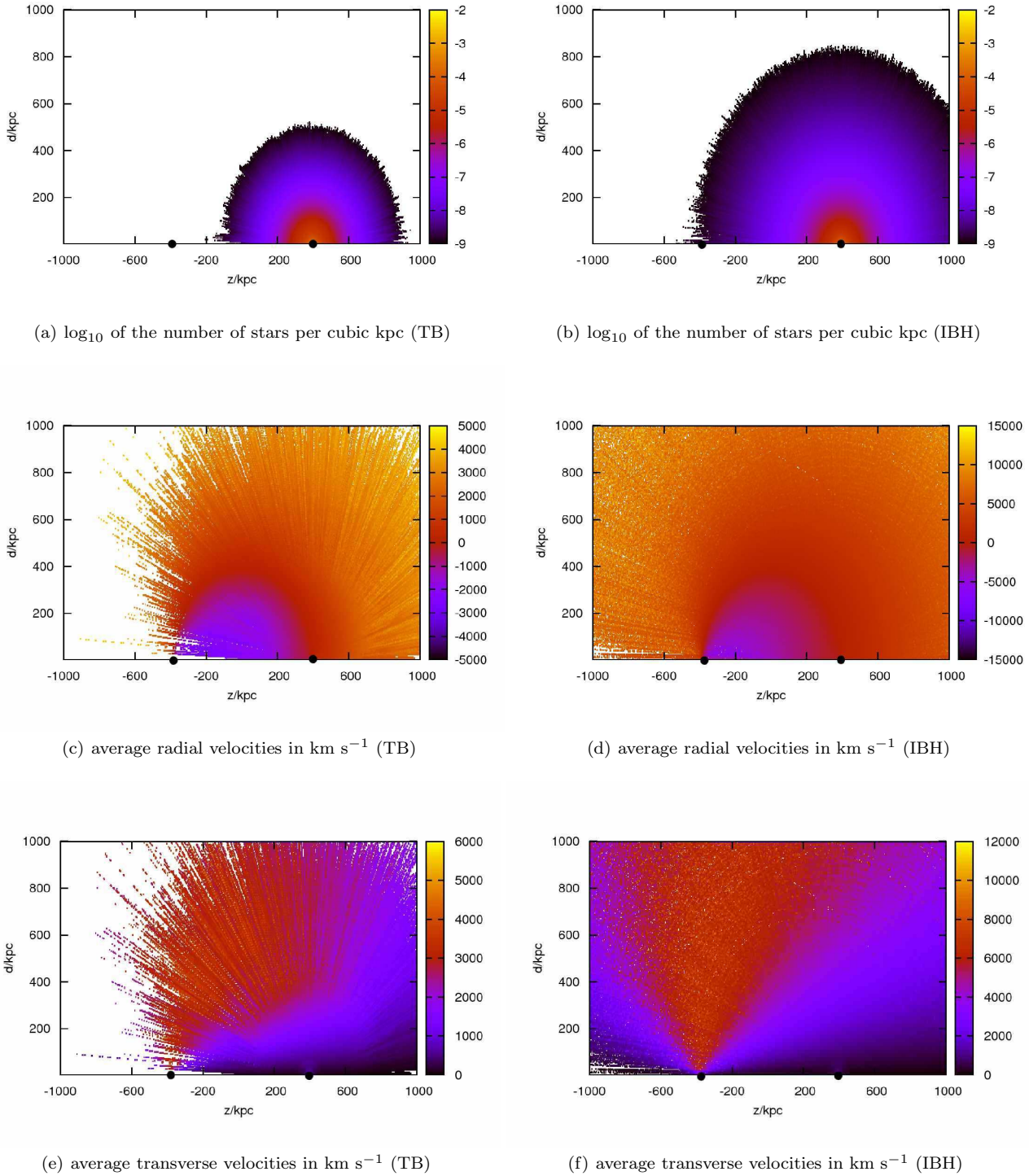


Figure 5. Same as Fig. 2 for stellar masses above $3M_{\odot}$.

4.3 HVS Velocities

We now consider the stellar velocities measured relative to the MW centre. It must be noted when considering M31 HVSs close to the Earth that we have neglected the MW bulge and disc, so that the actual M31 HVS velocities there will be somewhat higher than we depict in our plots.

We first describe our results for the TB mechanism. Figure 2 shows that for the first mass bin the radial and transverse speeds near the MW are typically $\approx 400 \text{ km s}^{-1}$. It is noticeable that the typical speeds of higher mass stars near the MW were substantially greater. For the third mass bin (Fig. 3) the typical velocity is $\approx 500 \text{ km s}^{-1}$ near the MW; for the fifth mass bin (Fig. 4) it is $\approx 700 \text{ km s}^{-1}$. The

high mass stars in Figure 5 appear to have particularly high velocities of $\approx 3000 \text{ km s}^{-1}$ near the MW, but of course the density of such stars is negligible in the regions where the speeds are so high.

The velocities resulting from the IBH mechanism (Figs. 2, 3, 4; right column) were significantly higher than for the TB mechanism, with typical speeds near the MW of 600 km s^{-1} , 800 km s^{-1} , 1000 km s^{-1} for the first, third and fifth mass bins respectively.

In all velocity plots the average velocities were larger at greater distances from the centre of M31 (though the numbers of HVSs there were smaller). The highest radial speeds occur near the intergalactic axis, whereas the highest transverse speeds can be found perpendicular to this axis as expected.

5 DISCUSSION

In our investigation, we found a chaotic sensitivity of the HVS trajectories to initial conditions. Chaotic regions of phase space are common for the motion of a test particle in a complicated three centre potential; chaos can even be found in non-stationary simple two body potentials, such as binary systems (see Holman & Wiegert 1999, Musielak et al. 2005).

The arc-like regions of raised density, which are seen for low mass stars with both ejection mechanisms, are due to the focusing of ejected HVSs by the MW’s gravitational field. The stars that are focused in this way by the MW have only just enough kinetic energy to escape the attraction of M31. They are thus very slow and spend a large amount of time in the observed “arc”, which leads to an increased density there, before falling back towards the intergalactic axis. While one expects regions of increased density, it is unclear why there is a sharp-featured substructure within the arc, as there are no sharp steps in the potential near this region. Such arc-like features are not observed for higher-mass stars. This follows from the reduced main-sequence lifetime of these stars ($t_l \propto m^{-2.5}$); high mass stars simply do not survive long enough to be visible along such long-lasting trajectories. The arcs are less pronounced for the IBH mechanism because it ejects HVSs at higher speeds, as can be seen from Equation (16).

It must be noted that the approximation of a static Local Group is not applicable to the longest-lasting trajectories. Taking the small initial separation of M31 and the MW into account would increase the number of low mass HVS from M31 we expect to find in the MW halo; the actual number densities of M31 HVSs in the MW may thus be higher than we calculate in Figure 2.

A large overdensity of stars was found near the intergalactic z -axis, which is also due to gravitational focusing. As described before, the gravity of the MW and the diffuse Local Group mass draw HVSs towards the intergalactic axis; the axial symmetry of the entire configuration means that every such trajectory eventually crosses the axis at some point, which increases the density there. It is important to note that this gravitational focusing has a very large effect; in Figure 2 it can be seen that it increases the number density of stars near the the MW by roughly *three orders of*

magnitude compared with the number of HVSs at an equal M31-distance off axis.

Of course, the real Local Group mass distribution will not be exactly axisymmetric. For instance, the symmetry of our model could be broken by the galactic discs, any triaxiality of the MW or M31 halo (see Gnedin et al. 2005), or by other Local Group galaxies. However, as the HVSs are usually moving very rapidly, their trajectories depend mainly on the large scale mass distribution. While local asymmetries may blur the axial overdensity somewhat, it is thus unlikely that they would eliminate this feature entirely.

The typical velocities of higher mass main-sequence stars are larger by selection; as more massive stars have shorter lifetimes, they require faster speeds to travel a certain distance within their lifetime. Similarly, HVSs have larger velocities at greater distances from M31 because only a star with a large velocity can reach a location far from M31 within its lifetime. The increased isotropy of the distribution of more massive stars is also due to the finite stellar lifetime: more massive stars are faster, faster stars are deflected less by the gravity of the Local Group, and less deflection implies a more isotropic distribution.

The forms of the radial and transverse velocity distributions are as expected for stars travelling away from M31. The shell-like minimum in the transverse velocity 300 kpc from M31 is due to many stars with velocities just below the escape velocity turning around at this radius.

6 OBSERVATIONAL OUTLOOK

We may now examine the observability of HVSs from M31 based on the results of our simulations. We first consider the large number of low mass ($\approx 1M_\odot$) stars expected within the MW halo, especially near the intergalactic axis. The total number density of low-mass stars is at least $\sim 10^{-3}/\text{kpc}^3$ in the MW halo. In a $\approx (100\text{kpc})^3$ survey volume in the MW halo one therefore expects ~ 1000 stars from M31. These stars have a number of features which distinguish them from the background MW stars. First, the metallicity of stars from galactic nuclei is different from stars in other regions of the galaxy. Second, the HVSs from M31 have much larger typical speeds than other stars in the MW halo. Their average radial speeds near the MW are at least 400 km s^{-1} (TB) and 600 km s^{-1} (IBH); however, some of these stars will of course have significantly larger speeds. In contrast to HVSs originating in the MW, many M31 HVSs will be moving *towards* the galaxy centre (on the side of the MW which faces M31, which is where the solar system is located) with radial speeds significantly exceeding the MW escape velocity. However, there is of course a contrast problem in observing such M31 HVSs, as the MW contains a very large number of $\sim 1M_\odot$ stars. A targeted spectroscopic search would probably be unfeasible. However, it may be possible to detect these HVSs in planned large scale surveys using telescopes such as Pan-STARRS, the Large Synoptic Survey Telescope or the planned *Global Astrometric Interferometer for Astrophysics* (GAIA) satellite. These surveys will measure proper and radial motions of $1M_\odot$ stars out to at least 10kpc (Perryman 2002, Yu & Tremaine 2003) and they should thus find a small number (~ 10) of M31 HVSs. Even a few stars with sufficiently large negative radial velocities or transverse

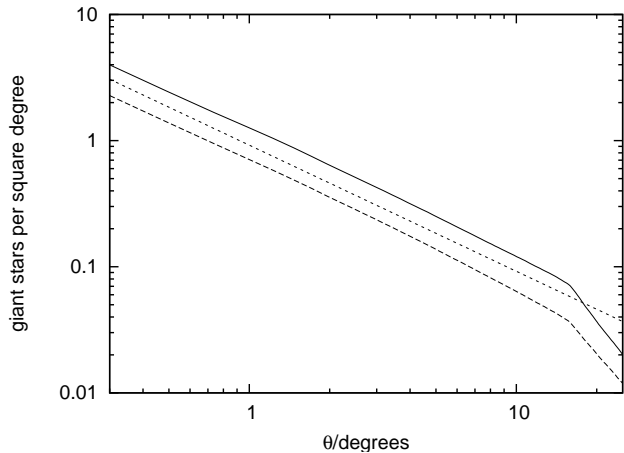


Figure 6. The number of luminous hypervelocity RGB stars per square degree within the distance range of 600–1000kpc from the MW, as a function of the angle from the centre of M31. Solid line: TB mechanism; long-dashed line: IBH mechanism; short-dashed line: for comparison, $0.92 \times (\theta/\text{degrees})^{-1}$ stars per square degree. One degree spans a distance of 13.6 kpc near M31.

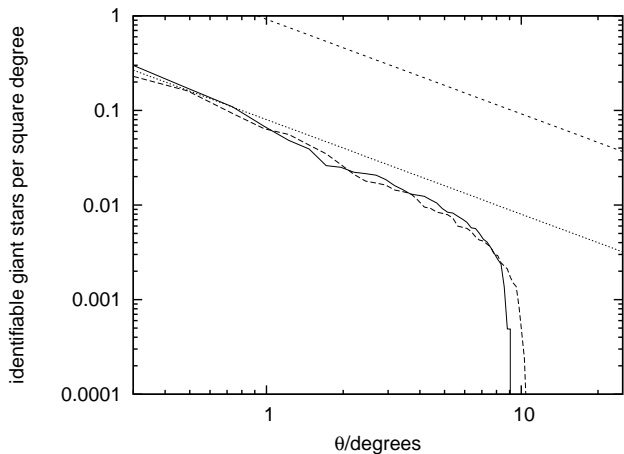


Figure 7. Same as in Fig. 6 but for identifiable hypervelocity RGB stars with radial approach velocities $< -420 \text{ km s}^{-1}$. Solid line: TB mechanism; long-dashed line: IBH mechanism; dotted line: for comparison, $0.08 \times (\theta/\text{degrees})^{-1}$ stars per square degree; short-dashed line: $0.92 \times (\theta/\text{degrees})^{-1}$ as in Fig. 6.

velocities would imply a HVS production in M31. Any such detection would be evidence against the BHC mechanism and could constrain the characteristics of the M31 galactic centre environment as well as the Local Group mass distribution. One could perhaps also distinguish between stars from the IBH and TB mechanisms by their measured velocities; high velocity HVSs produced by the IBH mechanism would indicate that the M31 MBH has an intermediate mass black hole companion (which may be difficult to detect by other means).

The current population of MW HVSs was discovered by observations of luminous main-sequence blue stars in the MW halo. From Figure 5, it is clear that the density of $> 3M_{\odot}$ HVSs from M31 is only significant close to M31 due to the stars’ short lifetime. Even massive $3 - 8M_{\odot}$ main sequence HVSs would be too faint to be observed near M31

(unevolved $3M_{\odot}$ blue have an apparent V magnitude of ≈ 24 at the distance of M31). Main sequence HVSs of masses greater than $\approx 8M_{\odot}$ may be detectable in M31, but one would expect only ~ 1 such ejected star to exist at the present time (it would be close to the M31 galactic centre). An observation of such a HVS would thus be very difficult.

However, there may be another possibility to detect more distant HVSs⁴. Stars with masses over $1M_{\odot}$ brighten to $\sim 10^3 L_{\odot}$ for about 5×10^6 years when they reach the tip of the red-giant-branch (RGB) (Schaller et al. 1992); the luminosity of these stars would make them observable to very large distances. For instance, such a star near M31 has an apparent V magnitude of ~ 21.5 and is thus bright enough to investigate spectroscopically. We calculated the distribution of such giant HVSs (as for the main sequence HVSs) and found that due to the short duration of the giant phase, significant densities of RGB HVSs could only be found within ~ 200 kpc of M31.

To examine the possibility of observing such RGB HVSs in the M31 halo, we constructed Figure 6, which depicts the density of hypervelocity red-giant-branch-tip stars per square degree as a function of the angular separation θ from M31 (along with an analytic fit to the results). The angular density of these stars is seen to fall off as $1/\theta$ at small angles; for $\theta > 15^{\circ}$ the density drops off more rapidly due to the finite stellar lifetimes. Significant numbers of RGB HVSs can be found at angles beyond the galactic disc and bulge ($> 1^{\circ}$), with ~ 70 (TB mechanism) or ~ 30 (IBH mechanism) hypervelocity RGB stars in the M31 halo at angles of $1^{\circ} \leq \theta \leq 10^{\circ}$. However, to distinguish such HVSs from background M31 halo stars and from MW foreground stars, they need to have radial approach velocities of $< -420 \text{ km s}^{-1}$ (the velocity dispersion of halo stars is less than $\approx 140 \text{ km s}^{-1}$, see Chapman et al. 2006). The angular density of such identifiable RGB HVSs is depicted in Figure 7; their density is roughly a factor of ten lower, so that one could find ~ 5 such giant stars within the M31 halo ($1^{\circ} \leq \theta \leq 10^{\circ}$). The background density of non-HVS RGB stars in M31 (Ibata et al. 2007, Fig. 18) is approximately four orders of magnitude greater than that of the HVS giants for $\theta > 1^{\circ}$. A number of studies of the M31 halo population have recently been performed, in which spectra of thousands of M31 halo giants have been obtained (e.g. Chapman et al. 2006, Ibata et al. 2007). Hypervelocity red giant stars could be detected in similar future surveys of stars near M31.

It should also be noted that the larger dwarf galaxies in the Local Group (e.g. M32 or the Large Magellanic Cloud) could also produce HVSs if they have central MBHs. This is consistent with the observation by Edelmann et al. (2005) of a HVS apparently coming from the Large Magellanic Cloud (see Gualandris & Portegies Zwart 2007). Calculations of the expected dwarf galaxy HVS production rates and HVS distributions are beyond the scope of this paper but would be interesting to investigate in future work. HVSs from dwarf galaxies could be distinguished from those from M31 by their speed and the direction of their motion.

⁴ We are grateful to Nelson Caldwell for this suggestion.

7 CONCLUSIONS

In this paper we have investigated the distributions and velocities of the hypervelocity stars from the M31 Galaxy by integrating a large number of star trajectories within the Local Group. Below we summarise the main conclusions from our calculations:

- The differences between the galactic centres of M31 and the MW imply that the BHC model for HVS production would not be effective in M31. The TB mechanism and the IBH mechanism could produce large numbers of HVSs in M31.
- Most HVSs ejected from M31 escape the local group, though some stars with lower velocities are gravitationally drawn towards the MW. The HVS trajectories show chaotic behaviour in some regions of phase space.
- While high mass stars can only be found close to M31, there are large numbers of low mass ($\approx 1M_{\odot}$) M31 HVSs on the intergalactic axis and in an arc near the MW. These significant overdensities close to the MW are caused by gravitational focusing. For both the TB and IBH mechanisms, we expect there to be a few thousand M31 HVSs within the virialized halo of the MW galaxy. These HVSs from M31 could be distinguished from other stars by their large radial approach velocities ($\sim -500 \text{ km s}^{-1}$) and could thus be detected by future large scale astrometric surveys.
- Our calculations of the number density of luminous hypervelocity RGB stars indicate that there are $\sim 30-70$ such stars in the M31 halo, of which ~ 5 should be identifiable and observable.

ACKNOWLEDGMENTS

We are very grateful to Warren Brown for many helpful discussions and useful comments on the manuscript. We thank Nelson Caldwell for interesting discussions and Donald Lynden-Bell for comments on the paper. BDS would like to acknowledge the support of the SAO intern program. This work was supported in part by NSF, Harvard University and FQXi funds.

REFERENCES

- Alexander, T., & Sternberg, A. 1999, *ApJ*, 520, 137
- Baumgardt, H., Gualandris, A., & Portegies Zwart, S. 2006, *MNRAS*, 372, 174
- Bender, R., et al. 2005, *ApJ*, 631, 280
- Binney, J., & Tremaine, S. 1987, *Galactic Dynamics*, Princeton, NJ, Princeton University Press
- Bromley, B. C., Kenyon, S. J., Geller, M. J., Barcikowski, E., Brown, W. R., & Kurtz, M. J. 2006, *ApJ*, 653, 1194
- Brown, W. R., Geller, M. J., Kenyon, S. J., & Kurtz, M. J. 2005, *ApJ*, 622, L33
- Brown, W. R., Geller, M. J., Kenyon, S. J., & Kurtz, M. J. 2006a, *ApJ*, 640, L35
- Brown, W. R., Geller, M. J., Kenyon, S. J., & Kurtz, M. J. 2006b, *ApJ*, 647, 303
- Brown, W. R., Geller, M. J., Kenyon, S. J., Kurtz, M. J., & Bromley, B. C. 2007, *ApJ*, 660, 311
- Chapman, S. C., Ibata, R., Lewis, G. F., Ferguson, A. M. N., Irwin, M., McConnachie, A., & Tanvir, N. 2006, *ApJ*, 653, 255
- Cohn, H., & Kulsrud, R. M. 1978, *ApJ*, 226, 1087
- Cox, T. J., & Loeb, A. 2007, ArXiv e-prints, 705, arXiv:0705.1170
- Edelmann, H., Napiwotzki, R., Heber, U., Christlieb, N., & Reimers, D. 2005, *ApJ*, 634, L181
- Eisenhauer, F., et al. 2005, *ApJ*, 628, 246
- Fich, M., & Tremaine, S. 1991, *ARA&A*, 29, 409
- Frank, J., & Rees, M. J. 1976, *MNRAS*, 176, 633
- Genzel, R., et al. 2003, *ApJ*, 594, 812
- Ginsburg, I., & Loeb, A. 2006, *MNRAS*, 368, 221
- Gnedin, O. Y., Gould, A., Miralda-Escudé, J., & Zentner, A. R. 2005, *ApJ*, 634, 344
- Gualandris, A., Portegies Zwart, S., & Sipior, M. S. 2005, *MNRAS*, 363, 223
- Gualandris, A., & Portegies Zwart, S. 2007, *MNRAS*, 376, L29
- Heacox, W. D. 1998, *AJ*, 115, 325
- Hernquist, L., & Quinn, P. J. 1989, *ApJ*, 342, 1
- Hernquist, L. 1990, *ApJ*, 356, 359
- Hills, J. G. 1988, *Nature*, 331, 687
- Hirsch, H. A., Heber, U., O’Toole, S. J., & Bresolin, F. 2005, *A&A*, 444, L61
- Holman, M. J., & Wiegert, P. A. 1999, *AJ*, 117, 621
- Ibata, R., Martin, N. F., Irwin, M., Chapman, S., Ferguson, A. M. N., Lewis, G. F., & McConnachie, A. W. 2007, ArXiv e-prints, 704, arXiv:0704.1318
- Kahn, F. D., & Woltjer, L. 1959, *ApJ*, 130, 705
- Kippenhahn, R., & Weigert, A. 1990, *Stellar Structure and Evolution*, Springer-Verlag Berlin
- Kormendy, J., & Bender, R. 1999, *ApJ*, 522, 772
- Klypin, A., Zhao, H., & Somerville, R. S. 2002, *ApJ*, 573, 597
- Lauer, T. R., et al. 1993, *AJ*, 106, 1436
- Levin, Y. 2006, *ApJ*, 653, 1203
- Lightman, A. P., & Shapiro, S. L. 1977, *ApJ*, 211, 244
- Loeb, A., Reid, M. J., Brunthaler, A., & Falcke, H. 2005, *ApJ*, 633, 894
- Lu, Y., Yu, Q., & Lin, D. N. C. 2007, ArXiv e-prints, 707, arXiv:0707.1872
- Lynden-Bell, D. 1967, *MNRAS*, 136, 101
- Magorrian, J., & Tremaine, S. 1999, *MNRAS*, 309, 447
- Maness, H., et al. 2007, ArXiv e-prints, 707, arXiv:0707.2382
- McConnachie, A. W., Irwin, M. J., Ferguson, A. M. N., Ibata, R. A., Lewis, G. F., & Tanvir, N. 2005, *MNRAS*, 356, 979
- Miller, M. C., Freitag, M., Hamilton, D. P., & Lauburg, V. M. 2005, *ApJ*, 631, L117
- Miralda-Escudé, J., & Gould, A. 2000, *ApJ*, 545, 847
- Musielak, Z. E., Cuntz, M., Marshall, E. A., & Stuit, T. D. 2005, *A&A*, 434, 355
- Navarro, J. F., Frenk, C. S., & White, S. D. M. 1996, *ApJ*, 462, 563
- O’Leary, R. M., & Loeb, A. 2006, ArXiv Astrophysics e-prints, arXiv:astro-ph/0609046
- Park, S. K., & Miller, K. W., 1988, *Communications of the ACM*, vol. 31, pp. 1192-1201
- Peebles, P. J. E., Melott, A. L., Holmes, M. R., & Jiang, L. R. 1989, *ApJ*, 345, 108
- Peebles, P. J. E. 1994, *ApJ*, 429, 43
- Peebles, P. J. E., Phelps, S. D., Shaya, E. J., & Tully, R. B. 2001, *ApJ*, 554, 104
- Perets, H. B., Hopman, C., & Alexander, T. 2007, *ApJ*, 656, 709
- Perryman, M. A. C. 2002, *EAS Publications Series*, 2, 3
- Press, W. H., Teukolsky, S. A., Vetterling, W. T., & Flannery, B. P. 1992, *Cambridge: University Press*, —c1992, 2nd ed.,
- Ribas, I., Jordi, C., Vilardell, F., Fitzpatrick, E. L., Hilditch, R. W., & Guinan, E. F. 2005, *ApJ*, 635, L37
- Sawa, T., & Fujimoto, M. 2005, *PASJ*, 57, 429
- Schaller, G., Schaerer, D., Meynet, G., & Maeder, A. 1992, *A&AS*, 96, 269
- Seigar, M. S., Barth, A. J., & Bullock, J. S. 2006, ArXiv Astrophysics e-prints, arXiv:astro-ph/0612228

- Sesana, A., Haardt, F., & Madau, P. 2006, ApJ, 651, 392
Sesana, A., Haardt, F., & Madau, P. 2007a, MNRAS, L53
Sesana, A., Haardt, F., & Madau, P. 2007b, ApJ, 660, 546
Valtonen, M. J., Byrd, G. G., McCall, M. L., & Innanen, K. A.
1993, AJ, 105, 886
Verlet, L. 1967, Phys. Rev. 159, 98
Widrow, L. M., & Dubinski, J. 2005, ApJ, 631, 838
Young, P. 1980, ApJ, 242, 1232
Yu, Q., & Tremaine, S. 2003, ApJ, 599, 1129